Heliyon 5 (2019) e01831

Contents lists available at ScienceDirect

Heliyon

journal homepage: www.heliyon.com

Investigations on the enhanced dye degradation activity of heterogeneous $BiFeO_3$–$GdFeO_3$ nanocomposite photocatalyst

Yathavan Subramanian [a], Venkatapathy Ramasamy [a], R.J. Karthikeyan [b], Gokul Raj Srinivasan [c], Durairajan Arulmozhi [d], Ramesh Kumar Gubendiran [a,*], Mohan Sriramalu [e]

[a] Department of Physics, University College of Engineering Arni, Anna University, India
[b] Department of Metallurgical and Materials Engineering, IIT Roorkee, Roorkee, India
[c] Department of Physics, C. Kandaswami Naidu College for Men, Chennai, India
[d] I3N-Aveiro, Department of Physics, University of Aveiro, Portugal
[e] Department of Physics, S.A. Engineering College, Avadi, Chennai, India

ARTICLE INFO

Keywords:
Materials science
Methylene blue dye
Photocatalysis
Nanocomposites
Ceramics
Nanomaterials
Photoluminescence

ABSTRACT

Perovskite types of nanocomposites of $BiFeO_3$–$GdFeO_3$ (BFO-GFO) has been synthesized using sol-gel route for the first time. The nanocomposite powders were characterized by powder X-Ray diffraction (PXRD) to confirm the existence of mixed crystallographic phases. EDX analysis on nanocomposites estimates the composition of individual element present in BFO-GFO matrix. The induced strain upon loading $GdFeO_3$(GFO) in $BiFeO_3$ (BFO) matrix has been computed with the aid of Williamson –Hall (W–H) plot. Surface morphologies of nanocomposite powders has been studied using Field Emission Scanning Electron Microscope (FESEM) images. The observed changes in the band gap energies of nanocomposite powders due to the inclusion of GFO has been ascertained from the tauc plots. PL emission of BFO upon loading GFO found to have detected in the IR region due to defect level transition. Finally, the methylene blue dye (MB) degradation characteristics of BFO, GFO and the nanocomposite powders of BFO-GFO have also been studied. The overall results obtained has been discussed in detail.

1. Introduction

Photocatalysis reactions have been extensively used for wastewater treatment [1,2]. The photocatalytic oxidation techniques were found to be best method to solve the environmental water pollution issues and energy crisis problems [3,4]. Wide band gap semiconductors like TiO_2, titanates, etc., were found to show high photocatalytic activity to the breakdown of organic compounds only within UV regime [5,6] and it has better stability, low cost, and non-toxicity. To improve the utilization efficiency of sunlight radiation and also to enhance the photocatalytic activity, fresh visible-light-driven photocatalysts with high photocatalytic activity and stability has to be designed [7, 8, 9, 10, 11]. Through a variety of reports exist in the literature on visible light photocatalysis [12, 13, 14, 15, 16, 17, 18, 19, 20, 21, 22, 23], certain materials are more responsive to both UV and visible light. Among them, $BiFeO_3$ (BFO) is a well-familiar and an important semiconductor photocatalyst because of its huge response to solar radiation, band gap and high stability [24, 25, 26, 27]. With these unique properties, $BiFeO_3$ (BFO) is identified not only as a visible light active photocatalyst, but also a potential material in solar and fuel cell applications. However, photocatalytic activity of $BiFeO_3$ (BFO) is still restricted due to the rapid recombination of electron and holes charge carriers and the conduction band (CB) electrons cannot be efficiently catched fully by O_2 to produce a lower surface area and to yield superoxide radicals. It is not very easy for a photocatalyst, based on a single metal oxide semiconductor to satisfy all needs such as stability, chemical inertness and reduced-recombination rate. Therefore, Photocatalyst based on combination of two semiconductors have been developed to increase photocatalytic character. In particular, Heterogeneous photocatalyst with wide band gap and high electric conductance semiconductor could provide a larger surface area and has shown improved dye degradation performance [28]. $BiFeO_3$ based heterogeneous photocatalyst including $BiFeO_3$/g-C_3N_4, $BiFeO_3$/-CuO, $BiFeO_3$/WO_3, $BiFeO_3$/Pt [29, 30, 31, 32, 33] substantiates the significances of photocatalytic activity of $BiFeO_3$ based compounds. For example, $BiFeO_3$/$ZnFe_2O_4$nanostructures exhibit excellent photocatalytic activity for degradation of methylene blue which has been ascribed for the improved visible-light absorption, charge carrier separation and migration [36]. Above all $BiFeO_3$ heterojunction

* Corresponding author.
E-mail addresses: smoh14@rediffmail.com, rameshvandhai@gmail.com (R.K. Gubendiran).

https://doi.org/10.1016/j.heliyon.2019.e01831
Received 22 November 2018; Received in revised form 26 April 2019; Accepted 23 May 2019

photocatalyst systems could show better photocatalytic performance for the photo-degradation of organic dye in aqueous medium, but its ability is slendered due to the rapid charge recombination. Researchers have modified the band energy positions of $BiFeO_3$ by the inclusion of high bandgap semiconductor catalysts to reduce the time of recombination of electron-hole pairs and thereby increasing surface area towards enhancing its photocatalytic activity. In particular, rare earth perovskite oxides with wide bandgap and visible light active semiconductor catalysts could provide a larger surface area and has shown improved photocatalytic cavity. Especially, $GdFeO_3$ (GFO) is a kind of typical rare-earth perovskite oxide, with a steady crystal structure and possess distinct characteristics of optical absorption and photocatalytic activity. It is visible light active semiconductor with a narrow band gap (2.3 eV) [35, 36, 37]. Due to its low density, high stability, non-toxicity, chemical inertness and largescale productivity, it has drawn wide attention to researches for using in various applications such as photoelectric devices, photovoltaic solar cell and photocatalysis [38,39]. Further, its high localized conductivity, low recombination rate and high specific surface area could also increase its overall photocatalytic efficiency in the event of loading with $BiFeO_3$. It is also worth noting that $GdFeO_3$ has suitable band edges that could well matches with $BiFeO_3$ band edges to form a direct solid-state Z scheme photocatalytic system, where the photogenerated electrons in conduction band of $BiFeO_3$ will exhibit strong reducibility and the holes in valence band of $GdFeO_3$ will present strong oxidizability. Hence, the combination of two visible light active semiconductors can become an efficient heterogeneous type of photocatalyst with improved visible light harvesting property and in turn can exhibit improved photocatalytic activity with greater stability. With this intention an attempt is made to develop a distinct and sustainable visible light induced $BiFeO_3$/$GdFeO_3$ heterojunction nanomaterial. To the best of our survey there are no much reports on the photocatalytic degradation of methylene blue dye using $BiFeO_3$/$GdFeO_3$ heterojunction photocatalyst.

2. Experimental

All the used chemicals were of analytical grade (AR) and used as received without further purification. The precursors were Bismuth Nitrate Penta hydrate (Merck- 99 % Purity), Iron Nitrate Nano hydrate (Merck -98% Purity), Conc. HNO_3 (Merck- 69%), Tartaric acid (Merck – 99%), Gadolinium Nitrate Hexa hydrate (Sigma Aldrich – 99%), Ethylene glycol (Merck – 99%).

2.1. Synthesis of $BiFeO_3$ nanoparticles

$BiFeO_3$ nanoparticles have been synthesized by Sol-Gel method through the literature reviews [40,41]. In a typical synthesis process, 3mmol of Bismuth Nitrate Penta hydrate & 3 mmol of Iron Nitrate Nano hydrate dissolved in 50ml of Distilled water. 3ml of Conc. HNO_3 & 3 mmol of Tartaric acid were added along with above solution and stirred gently at 115 °C till it turns into Brownish solid solution. The obtained solution was enabled for drying at the temperature of 150 °C to get brownish dry powders. Upon drying the brown powders were calcined in furnace at 500 °C for 2 h to get phase pure $BiFeO_3$ Nanopowders.

2.2. Synthesis of $GdFeO_3$ nanoparticles

$GdFeO_3$ nanoparticles were synthesized through glycol-assisted sol−gel technique [30]. 15 mmol of Gadolinium Nitrate Hexa hydrate were mixed with in 40 mL of Ethylene glycol to get a transparent solution. Then, 15 mmol of Ferric Nitrate Nona hydrate [$Fe(NO_3)_3{\cdot}9H_2O$] was added into the above solution. After stirring continuously for 4 h along with heating at 110 °C, a brownish red colloidal mixture was obtained. The sol was dried at 120 °C for 8 h and the obtained $GdFeO_3$based xerogel was precalcined at 450 °C for 0.5 h to remove NO_3^- and organic compounds. The remaining powders were heated in furnace at 800 °C for 4 h so as to obtain pure Nanopowders of $GdFeO_3$.

2.3. Synthesis of $BiFeO_3$-$GdFeO_3$Nanocomposites

$BiFeO_3$-$GdFeO_3$ nanocomposite has been prepared from Sol-Gel synthesis in accordance with previous literature [38]. Initially, 3mmol of Bi $(NO_3)_3.5H_2O$, 3 mmol of Fe $(NO_3)_3.9H_2O$ and 10 mg of $GdFeO_3$ were added in 50ml of Distilled water. 3ml of Conc. HNO_3 and 3mmol of Tartaric acid were then mixed to the above solution. Then the solution was heated at 115 °C with continuously stirring, till it changes into reddish brown solid solution. Subsequently, the solid solution was permitted for drying process at 150 °C to get dry powders. After drying, the reddish-brown powders were calcined at 500 °C for 2 h to get $BiFeO_3$-$GdFeO_3$ nanocomposite powders.

2.4. Photocatalytic test on $BiFeO_3$- $GdFeO_3$ nanocomposites

Photocatalytic activity of the $BiFeO_3$-$GdFeO_3$nanocomposite was investigated by the degradation of methylene blue (MB) in water under natural sunlight radiation. $BiFeO_3$ and $GdFeO_3$ were used as the photocatalytic reference to find the performance of the$BiFeO_3$-$GdFeO_3$ composite system. In each experiment, 10mg of photocatalyst was added to10 mL of methylene blue (MB) solution at the concentration rate10 mg/L. The dye and sample suspension were stirred in dark for 120 min so as to ensure the adsorption/desorption equilibrium. Then the solution was kept under natural sunlight. For every 3 hours interval, about 1.0 mL of degraded dye was sampled and it was separated from the aqueous solution by the way of centrifugation at 6000 rpm for 2 min. The concentration of each degraded solution was monitored.

2.5. Characterization techniques used for $BiFeO_3$-$GdFeO_3$ nanocomposites

Crystal structural analysis of $BiFeO_3$–$GdFeO_3$ photocatalysts was done using a 'X'PERT PANalytical' make powder X-ray diffractometer (PXRD) in the 2θ range 10º- 60º with a scan rate of 2º/min. Field emission scanning electron microscope (FESEM) images were recorded using S–3400N Hitachi microscope to study the morphologies of polycrystalline samples. The elemental compositions of the individual constituents Bi, Gd, Fe etc., have been found from Energy Dispersive X-ray analysis (EDX) analyzer. Electronic spectra of $BiFeO_3$, $GdFeO_3$ and $BiFeO_3$–$GdFeO_3$ have been recorded from JASCO V-670 spectrophotometer in the wavelength regime 200–800 nm. Fourier transform infrared spectroscopy (FTIR) spectra was recorded from KBr pellet method using Shimadzu IR Affinity -1 spectrophotometer in the frequency range400–4000 cm^{-1}. Dye degradation properties of the $BiFeO_3$–$GdFeO_3$ photocatalyst at regular intervals of time was analyzed with the aid of LAB INDIA double beam UV-Vis spectrophotometer (Mode no: U2900) in the wavelength range 200–800nm. The path length was fixed as 10 mm for all experimental trails.

3. Results and discussion

3.1. Powder XRD studies on $BiFeO_3$- $GdFeO_3$ nanocomposites

Fig. 1 shows the powder XRD patterns of the $BiFeO_3$, $GdFeO_3$ and the$BiFeO_3$–$GdFeO_3$ nanocomposites $BiFeO_3$ shows indexed diffraction peaks at 2θ = 32.1º and 2θ = 23.1º corresponding to a R3c space group of rhombohedral phase (JCPDS no. 72–2112) and it indicates the well crystallized $BiFeO_3$ phase produced from sol-gel method [42,43]. No other impurity phases were observed along with $BiFeO_3$phase. Well broadened peaks of $BiFeO_3$ typically shows the nanoparticles are in nano dimension. Similarly, in case of $GdFeO_3$, the indexed diffraction peaks at 2θ = 23.2º, 26.09º, 32.2º, 33.2º, 33.8º& 34.38º match well with the orthorhombic structure having Pbnm space group. It is also in good agreement with the standard JCPDS card no.00-047-0067 and other earlier reports [44,45]. All other peaks obtained for $GdFeO_3$have reflected only the orthorhombic signals and no other satellite peaks were found.

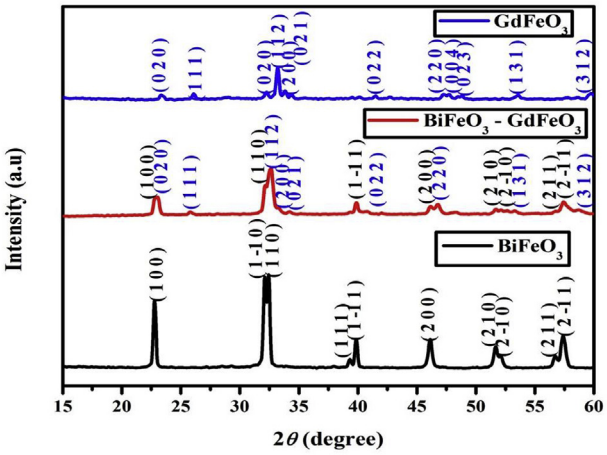

Fig. 1. Powder XRD patterns of $BiFeO_3$, $GdFeO_3$and nanocomposites of $BiFeO_3$–$GdFeO_3$.

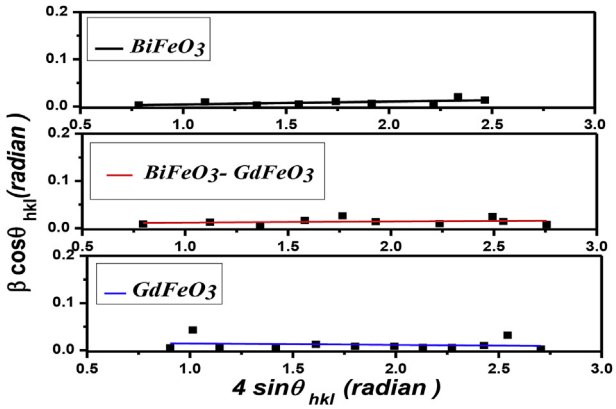

Fig. 2. W–H Plots of $BiFeO_3$, $GdFeO_3$and BFO-GFO nanocomposite powders.

In case of $BiFeO_3$ - $GdFeO_3$ composites, the $BiFeO_3$ diffraction pattern continued to be present but in broadened mode with low intensities due to the union of orthorhombic $GdFeO_3$ crystallites and it has also modulated the sizes of the $BiFeO_3$ nanoparticles and it is evidenced from the well-defined XRD peaks of $BiFeO_3$.

The average particle size of $BiFeO_3$ and $GdFeO_3$ calculated from Scherer formula were established to be ≈24 nm and 11 nm respectively in an isolated phase, whereas in composite phase, the average size crystallites of BFO & GFO dispersed in the size range 14–35 nm.

Upon compositing with $GdFeO_3$, the doublet diffraction peak of $BiFeO_3$around $2\theta = 32°$ and $2\theta = 23°$ found to have merged and it has confirmed that $GdFeO_3$ particles have homogenously got mixed along with $BiFeO_3$ powders. Further all the peaks of $BiFeO_3$ have a shifted towards lower 2θ values and it provides an additional clue for the formation of nanocomposite of $BiFeO_3$ - $GdFeO_3$. Similar kind of signature was obtained for $ZnFe_2O_4/BiFeO_3$ heterojunction. Furthermore, no other impurity peaks were appeared other than $BiFeO_3$ and $GdFeO_3$ and it indicates that $GdFeO_3$ has been successfully loaded on the $BiFeO_3$ particles without destroying its own crystal structure. The overall results confirmed that the heterogeneous $BiFeO_3$-$GdFeO_3$ photocatalyst could only be composed of rhombohedral $BiFeO_3$and orthorhombic structure of $GdFeO_3$.

In order to analysis the crystalline strain upon loading $GdFeO_3$ photocatalyst, Williamson–Hall (W–H) analysis [38] was carried out for $BiFeO_3$, $GdFeO_3$ and$BiFeO_3$ - $GdFeO_3$ nanocomposite samples. The induced strain and observed changes in crystallite sizes have been estimated using the formulae.

$$\beta_{hkl} = \left[(\beta_{hkl})^2_{measured} - (\beta_{hkl})^2_{instrumental}\right]^{\frac{1}{2}} \quad (1)$$

$$D = \frac{K\lambda}{\beta_{hkl}\, COS\, \theta} \quad (2)$$

$$\varepsilon = \frac{\beta_{hkl}}{4\, tan\, \theta} \quad (3)$$

$$\beta_{hkl} = \frac{K\lambda}{D\, cos\, \theta} + 4\varepsilon\, tan\, \theta \quad (4)$$

$$\beta_{hkl}\, cos\, \theta = \frac{K\lambda}{D} + 4\varepsilon\, sin\, \theta \quad (5)$$

where;

D - is the crystallite size.

K - is the shape factor (0.94).

λ - is the wavelength of Cukα radiation.

θ -is theBragg angle

β_{hkl} -is the Full width at half maximum &

ε–represents the Crystalline Strain.

The observed variation in the crystalline strain and average crystallite sizes for $BiFeO_3$, $GdFeO_3$and $BiFeO_3$ - $GdFeO_3$from W–H plots and are shown in Fig. 2. The value of 'ε' and 'β' for each sample is also listed in Table 1. The strain modulation of $BiFeO_3$ - $GdFeO_3$nanocomposite particles due to GFO inclusion has considerably influenced its crystallite sizes.

3.2. FESEM analysis on $BiFeO_3$ - $GdFeO_3$ nanocomposites

The surface morphologies of the $BiFeO_3$ and $GdFeO_3$ in $BiFeO_3$ - $GdFeO_3$ nanocomposite have been analysed using a scanning electron microscope. The Field Emission Scanning Electron Microscope (FESEM) micrographs of the $BiFeO_3$ - $GdFeO_3$ nanocomposites shown in Fig. 3(a). The white granular particles (clearly visible in between $BiFeO_3$) represent the $GdFeO_3$ particles and the quasi-spherical shapedsheet shows the presence of $BiFeO_3$ in the nanohybrid structure. The presence of hybrid phases in the same field of view confirmed the successful synthesis of nanohybrids of $BiFeO_3$ - $GdFeO_3$ from sol-gel route. The white granules of $GdFeO_3$ nanoparticles are found to be well scattered on the surface as well as on the edges of the $BiFeO_3$. The distribution of the $GdFeO_3$ nanoparticles was more homogeneous on the $BiFeO_3$ spherical sheets. However, agglomeration of the $GdFeO_3$ nanoparticles occurred during attachment onto the $BiFeO_3$ quasi-spherical shaped sheet. The agglomerated clumps of $GdFeO_3$ nanoparticles have irregular shapes and the agglomerate ratio increased with $GdFeO_3$ loading. Fig. 3 (b) shows the Energy Dispersive X-ray analysis (EDX) data indicating the composition of element present in the heterogeneous photocatalyst and it gives an additional confirmation to the presence of $GdFeO_3$ in the nanohybrid of $BiFeO_3$ - $GdFeO_3$system.

In the case of $BiFeO_3$ nanohybrid loaded with $ZnFe_2O_4$ using co-precipitation synthesis [46], it was found that $BiFeO_3$ exists as spherical particles and $ZnFe_2O_4$ was noticed as nanoplates. However, a strong interfacial coupling was observed between $ZnFe_2O_4$ and $BiFeO_3$. As similar kind of distinct feature in the morphology has been witnessed for $BiFeO_3$and $GdFeO_3$. The present formation of heterojunction would also

Table 1
Crystalline strain and crystallite sizes for BFO, GFO and BFO - GFO.

S. No	Name of the Photocatalyst	Crystallite Size (nm)	Strain
1	$BiFeO_3$	~24 nm	6.07 E-3
2	$GdFeO_3$	~11 nm	2.94 E-3
3	**$BiFeO_3$ -$GdFeO_3$**	~14–35 nm	2.29 E-3

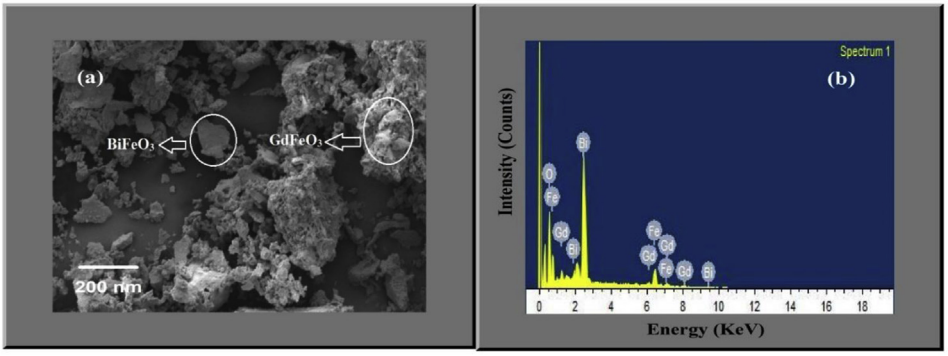

Fig. 3. (a) Dispersion of BFO and GFO nanoparticles in BFO-GFO nanocomposites (b) EDAX mapping of BFO-GFO nanocomposite powders.

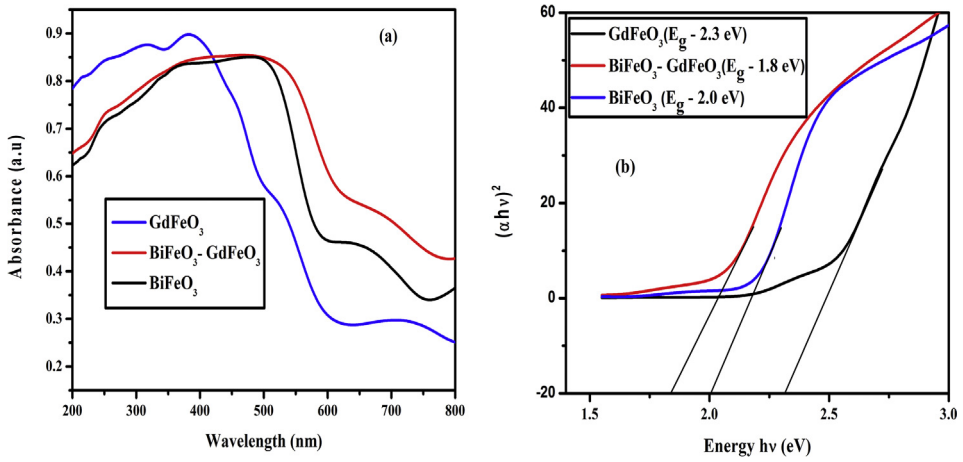

Fig. 4. (a) UV-Vis –NIR spectra of $BiFeO_3$, $GdFeO_3$ and BFO-GFO nanocomposite (b) Tauc plots representing the E_g values of $BiFeO_3$, $GdFeO_3$ and BFO-GFO nanocomposites.

have an appreciable figure of interfacial coupling. Therefore, there shall be ample chances for the facial migration of charge carriers (electrons and holes) in $BiFeO_3$ - $GdFeO_3$ based photocatalyst.

3.3. *UV-Vis-NIR studies on $BiFeO_3$ - $GdFeO_3$ nanocomposites*

Optical absorption properties on the synthesised samples of BFO-GFO was characterized by UV-Vis-NIR Spectra and it is shown in Fig. 4(a). $GdFeO_3$ mainly exhibits absorption in the UV wavelength range and its unique absorption edge is around ~390 nm. On the other hand, the optical absorption of $BiFeO_3$ lies at 500 nm. For $BiFeO_3$ - $GdFeO_3$ composites, they present significantly widen absorption area even beyond 530 nm and obviously makes the absorbance of the composites shifting towards longer wavelength side. This may perhaps due to the formation

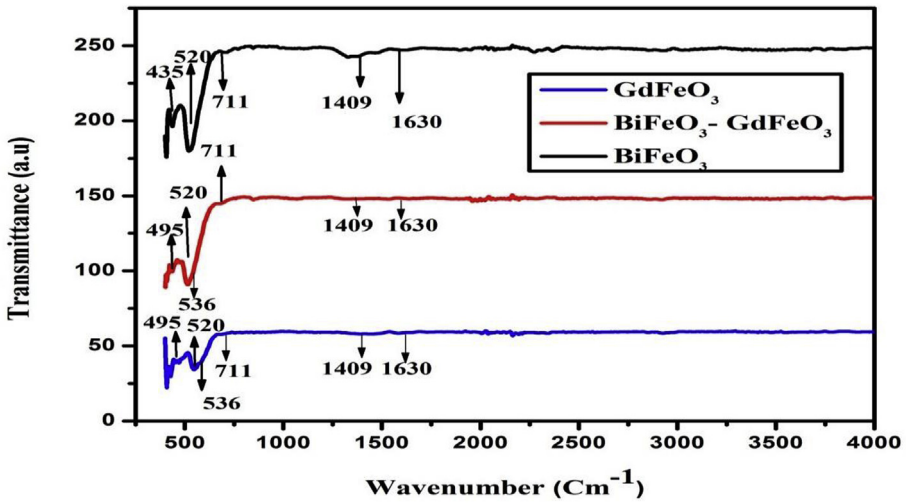

Fig. 5. FTIR spectra of $BiFeO_3$, $GdFeO_3$ and $BiFeO_3$–$GdFeO_3$ nanocomposite powders.

of tight chemical bonded surfaces between $BiFeO_3$and $GdFeO_3$. A fair broadening of absorption area upon addition of $GdFeO_3$ towards visible light region is quite similar to the ideology of D. Moitra et.al [47] in Graphene– BFO composites. Therein, it was pointed out that the change in absorption area upon loading a catalyst with $BiFeO_3$ is a key indicator for deciding the nature of chemical bonding. Therefore, the improvement in chemical bonding between BFO and GFO nanoparticles could be correlated from the absorption spectrum of the composite samples.

The energy band gaps of the $BiFeO_3$, $GdFeO_3$ and $BiFeO_3$ -$GdFeO_3$ samples were calculated using Kubelka-Munk function [48]. The calculated band gap values are 2.0 eV (BFO), 2.3 eV (GFO) and 1.8 eV (composite) and it is shown in Fig. 4(b). Thus, the introduction of $GdFeO_3$ on $BiFeO_3$ shows its ability to effectively narrow down the band gap of $BiFeO_3$ - $GdFeO_3$ composite which is due to the interaction and synergism between $BiFeO_3$ and $GdFeO_3$. The decrease in the band gap energy for $BiFeO_3$ -$GdFeO_3$ may be due to the fact that $GdFeO_3$ addition would possibly be decreasing electronic correlation energy with oxygen vacancies introduced by the valence state of Fe^{3+} ions. It is noteworthy to mention here that such significantly enhanced visible light absorption spectrum and lowering of band gap would be helpful for improving the photocatalytic performance.

3.4. *Vibrational structure analysis on $BiFeO_3$–$GdFeO_3$ nanocomposites*

FTIR patterns of $BiFeO_3$, $GdFeO_3$ and $BiFeO_3$–$GdFeO_3$ photocatalysts are shown in Fig. 5. The spectrum of $BiFeO_3$ indicates a two IR absorption peaks at ca.455 and 520 cm^{-1} corresponding to the overlapping Fe –O stretching and bending vibrations. It is also found as the characteristic absorption of FeO_6 octahedra of the perovskite structure [49]. A weak peak at ~711cm^{-1} for $BiFeO_3$ is assigned to the water absorption from the environment and it is also highlighted in the earlier report [50]. This peak has been found less pronounced in $BiFeO_3$-GdFeO3 composite. This would confirm that the hydroscopic property of the BFO-GFO nanocomposite sample is partially lower than the pure gadolinium ferrite

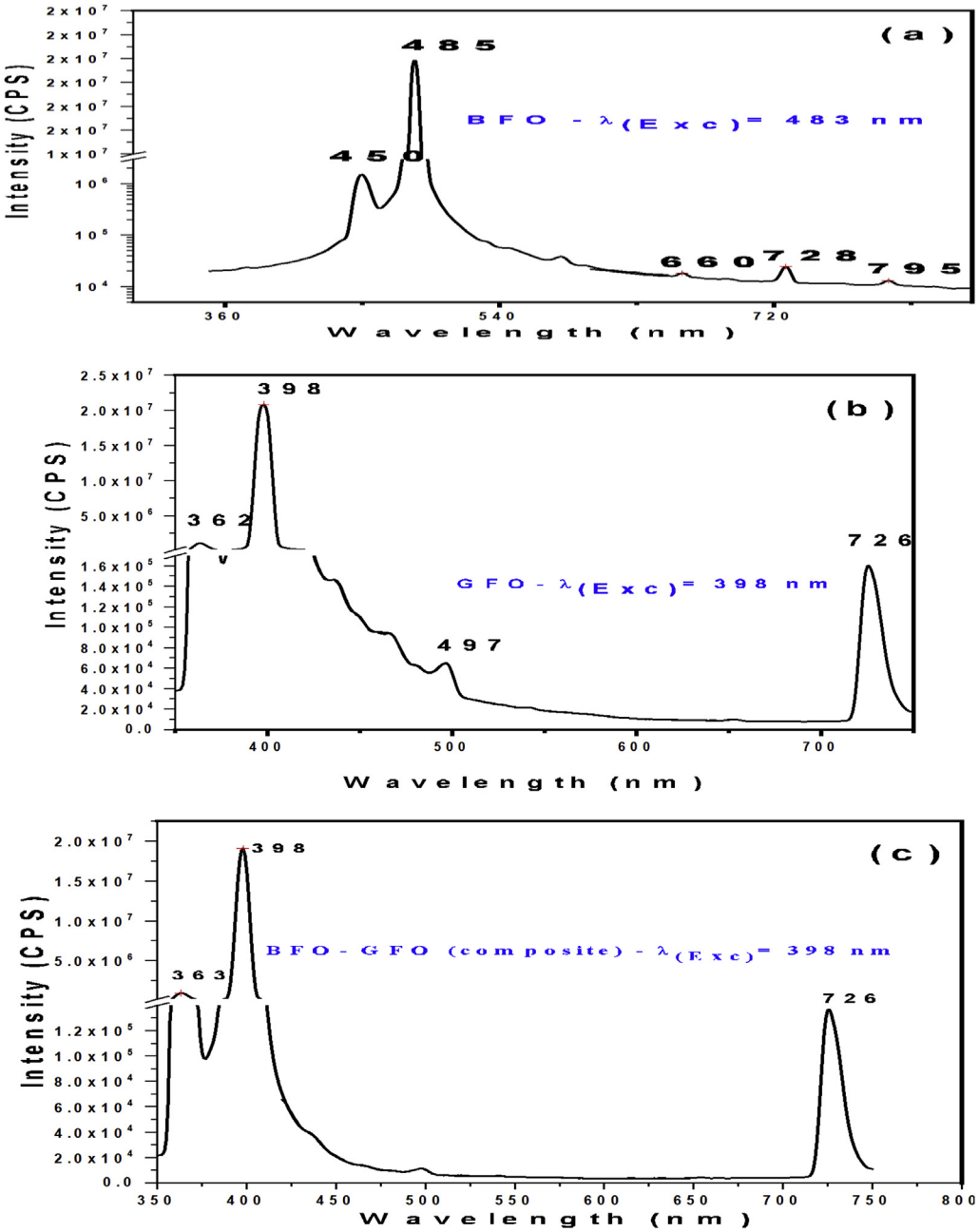

Fig. 6. PL emission spectra of (a) $BiFeO_3$, (b) $GdFeO_3$ and (c) $BiFeO_3$–$GdFeO_3$ nanocomposites.

molecules upon loading with BFO.

The medium IR absorptions in the range 3100–3600 cm^{-1} and the band at ~ 1620 cm^{-1} may be ascribed to υ(OH) and δ (H_2O) of water molecules absorbed on the photocatalyst surface. In case of $BiFeO_3$-$GdFeO_3$ nanocomposite, a new peak observed at ~536 cm^{-1} is due to the vibration of a Gd–O stretching vibration [51] and a peak at ~ 495 cm^{-1}has been attributed to the stretching vibrations of Gd-O-Gd in addition to the vibrations of $BiFeO_3$. The vibrational spectrum contains both the metal oxide vibrations of Gadolinium ferrite and Octahedral environment (FeO_6) of bismuth. The vibrational spectrum of the BFO-GFO composite corroborates with the results obtained from both power XRD and SEM images.

3.5. Photoluminescence (PL) studies on BFO – GFO nanocomposites

Room temperature PL spectra has been recorded for BFO, GFO and the composite powders of BFO-GFO by dispersing the particles in acetone and it is shown in Fig. 6. PL spectrum of $BiFeO_3$ (excited at λ = 483 nm) consists of two major emissions at 450 nm and 485 nm and three other feeble emissions could also be detected at 660, 728 and 795 nm. The

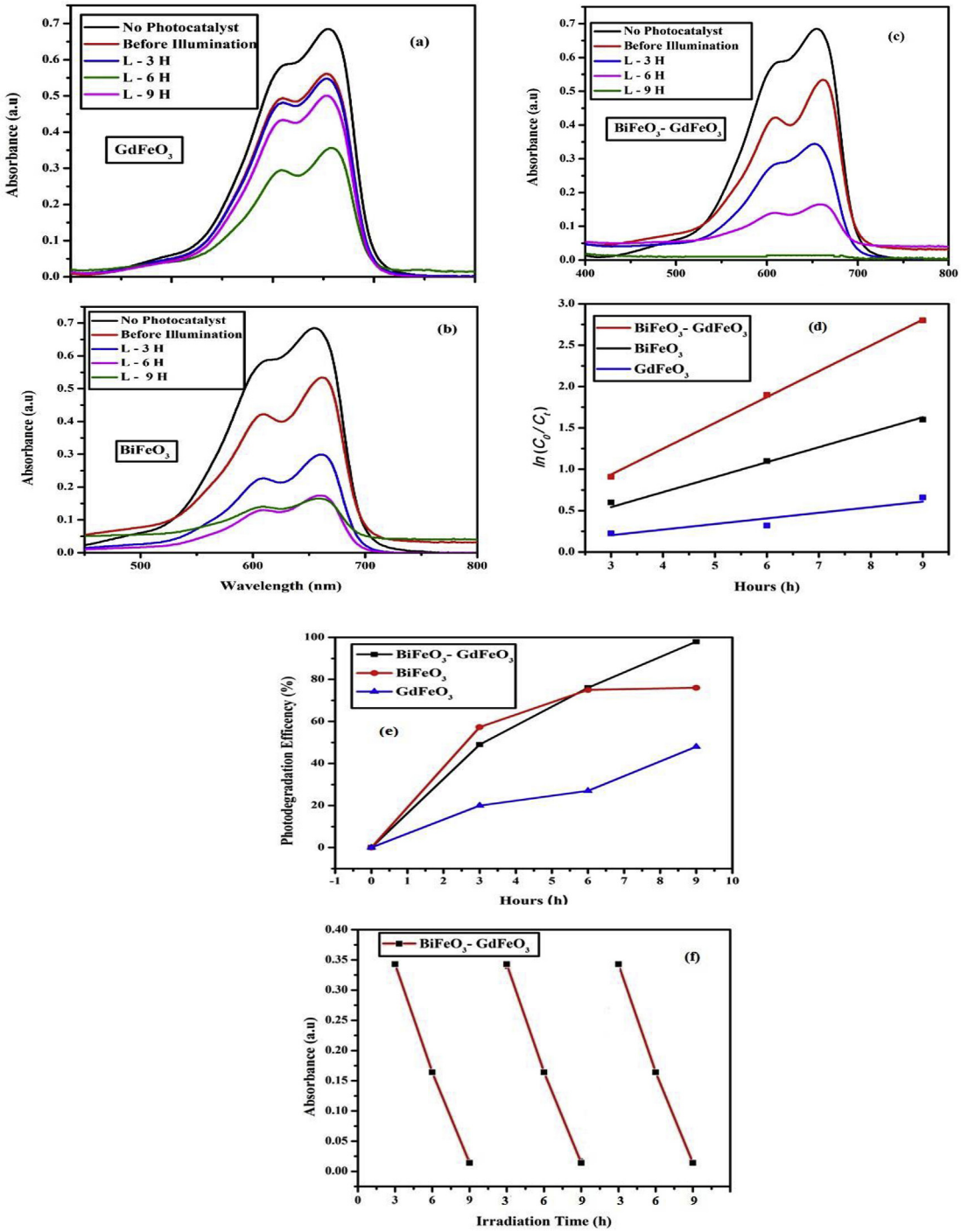

Fig. 7. (a) Wavelength Vs MB dye absorbance for (a) $GdFeO_3$, (b) $BiFeO_3$ suspensions (c) Wavelength Vs MB dye absorbance of $BiFeO_3$ - $GdFeO_3$ suspension (d) Exposure time Vs ln (C_0/C_t) for BFO, GFO and nanocomposites of BFO-GFO (e) Exposure time Vs Photo degradation efficiencies BFO, GFO and BFO-GFOnanocomposites (f) Reusability studies on Methylene blue dye absorbance of nanocomposite of BFO-GFO for every 3 hours interval.

emission peaks at 450 and 485 nm are related to the near band emission characteristics of BFO. The other weak signals arose due to defect level emissions. The origin of defects may be from oxygen vacancies in the crystal structure and surface area changes in the crystallites. In respect of $GdFeO_3$, the near band emissions occur at 362 and 398 nm. The defect induced emissions have also been detected at 497 and 726 nm. The blend of BFO and GFO nanocomposite powders has been excited at 398 nm. Apart from interband transitions, a strong emission peak towards the higher wavelength side at 726 nm (Red shift) and a weak shift towards the UV regime at 363 nm was also observed from the spectrum. Similar kind of observation was also witnessed in Gadolinium doped BFO [52]. It has been noticed that the inclusion of gadolinium ferrite in the BFO material has considerably enhanced the PL emission intensities especially at the higher wavelength of 726 nm and also the interband transition at 398 nm. This can also be ascertained from the PL emission of pure GFO material.

The increase in PL intensities in BFO-GFO composite both for the near band transition and defect induced non-radiative transition might have occurred due to these possible reasons (i) passivation of oxygen vacancies upon loading $GdFeO_3$(ii) substantial increase number of trapped electrons giving rise to additional electron made available in the heterojunction (BFO-GFO) interface. This will enhance the space charge separation regime and electrons from CB of $GdFeO_3$ to cause more junction layer diffusion. Similarly, holes diffuses from VB of BFO reaches the heterojunction. This results in the increase in PL intensities of BFO-GFO composite over the individual moieties consequent to the introduction of defect levels in the composite phase.

3.6. Photocatalytic dye degaradtion activity of $BiFeO_3$ –$GdFeO_3$ nanocomposites

The photo dye degradation efficiency of methylene blue (MB) dye for $BiFeO_3$, $GdFeO_3$ and $BiFeO_3$ –$GdFeO_3$ composites as a function of wavelength (nm) are summarized in Figs. 7(a), 7(b) & 7(c). Methylene blue was scarcely degraded by pure $GdFeO_3$ after 9 hr which showed its limited photocatalytic activity on MB under visible light. The low photodegradation efficiency of $GdFeO_3$ was confirmed due to its high band gap potential, UV light active absorption area and poor photoelectric conversion. In case of $BiFeO_3$, it can degrade upto 76% of MB after 9 hours of irradiation. The extraordinary MB photodegradation efficiency of 98% was observed for the $BiFeO_3$-$GdFeO_3$ composite after 9 hr of irradiation. Enhanced photocatalytic efficiency of the $BiFeO_3$-$GdFeO_3$ composite may be due to the formation of heterojunction, which could encourage photogenerated electron–hole pairs and thus causes for the enhanced photocatalytic activity. Another important reason for high photodegradation efficiency is due to its low band gap tuning and visible light response. However, the efficiency strongly depend only on the content of the two components in the composite and higher specific surface area would also adsorb more Methylene blue dye on the exterior of its particles. Hence it facilitates for the higher photodegradation of MB dye. In order to study the reaction kinetics of Methylene blue degradation, the pseudo-first-order equation according to Langmuir–Hinshelwood model [53] has been evaluated and it can be expressed by the equation,

$$\ln\left(\frac{C_0}{C_t}\right) = kt \tag{6}$$

Table 2
Comparison of rate constants for various photocatalysts with BFO – GFO and their corresponding goodness of fit values.

Estimated values of first order kinetic constants for BFO, GFOand BFO - GFO solution with methylene blue				
S.NO	Photocatalyst	Slope K (min^{-1})	Standard Error	R^2 Value
1.	BFO	0.18095	0.00412	0.99948
2.	GFO	0.06771	0.00644	0.97338
3.	BFO -GFO	0.31214	0.00246	0.99981

Table 3
Comparative analysis on the dye degradation efficiencies of few heterogeneous photocatalysts.

S. No	Name of Heterogeneous Catalyst	Degradation Efficiency (%)	Reaction condition	Dye used	Time (Hour)
1	SiO_2–WO_3 [56]	37%	Halogen lamp (72 W, 1520 lm) under visible light at room temperature	Methylene Blue (MB)	3
2	$BiFeO_3$/MOF nanocomposite [57]	48%	Visible light irradiation (Xe lamp, 300 W) in a catalyatic reactor at 20 °C	Methylene Blue (MB)	3
3	CuO–$BiVO_4$ [58]	40%	Visible-light irradiation (18-watt fluorescent light), Room temperature	Methylene Blue (MB)	3
4	$BiFeO_3$/$GdFeO_3$ (Present Work)	56%	Natural sunlight and at atmospheric temperature/ condition	Methylene Blue (MB)	3

where C_0 and C_t are the concentrations of MB (mg L^{-1}) at different irradiation time of *0* and *t* respectively. *'k'* is the pseudo-first-order rate constant of photodegradation (min^{-1}) of methylene blue (MB). From Fig. 7 (d), the linear fitting curves of *ln* (C_0/C_t) versus irradiation time *(t)* also confirmed the better correlation to pseudo-first-order reaction kinetics for BFO- GFO photocatalyst over the virgin ones. The first order kinetic constant value has been estimated for nanocomposite and virgin samples. The values of R^2have been tabulated in Table 2. Photocatalytic degradation efficiencies have also been calculated both for the parent and nanocomposite particles using Eq. (7).

$$Efficiency,\ \eta(\%) = \frac{(C_0 - C_t)}{C_0} * 100 \tag{7}$$

The variation in the efficiencies for BFO, GFO and BFO-GFO composite are is shown in Fig.7(e) and a comparative analysis on the dye degradation efficiencies of few heterogeneous photocatalyst with BFO - GFO has also been tabulated in Table 3.

The stability of $BiFeO_3$ –$GdFeO_3$ samples has been subjected to investigation for a consecutive trail run of 3 cycles @ 9 hours (h)/cycle to a total of 27 hours. The composite sample was confirmed to be more stable and it was found that the stability remains unchanged even at the 3rd run.

The photocatalyst recovered after every each cycle, with help of centrifugation from the aqueous medium has been dried in oven for 4 hours (h). Then the recovered nanocomposite samples can be reused again for the photo degradation of Methylene blue solution under natural sunlight for another 9 hour (h) run. This has been tested for 3 cycles. The absorbance values were found to remain unchanged in all observed cycles. The graph indicating reusability of composites is shown in Fig. 7(f).

3.7. Proposed mechanism of photocatalysis in$BiFeO_3$ –$GdFeO_3$ nanocomposites

The photocatalytic dye degradation mechanism can be defined using three main steps:

(1) Photon absorption over the surface of the photocatalyst;
(2) The generation of photo-generated electron-hole pairs and

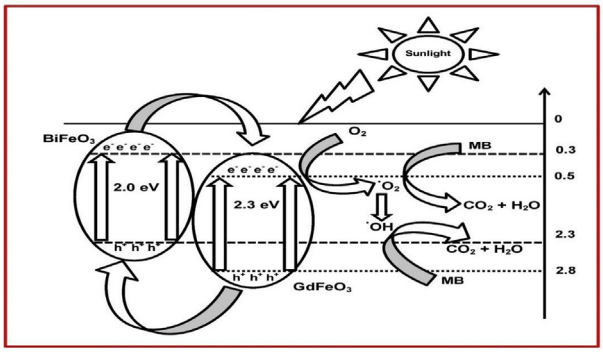

Fig. 8. Z-scheme representation of BFO-GFO nanocomposites.

(3) The dye adsorption photochemical reactions over the surface of the photocatalyst.

A schematic mechanism of the photocatalytic dye degradation of methylene blue using $BiFeO_3$ –$GdFeO_3$ nanocomposite is explained in Fig. 8. The electron and hole generation in the conduction band (CB) and valence band (VB) were totally depend upon band edge positions of the virgin $BiFeO_3$ and $GdFeO_3$. The valance band and conduction band positions for $BiFeO_3$ and $GdFeO_3$ were calculated using the Mullikan electronegativity method [54] as per the following steps.

$$E_{VB} = X + 0.5E_g - 4.5\ (Ee) \tag{8}$$

$$E_{CB} = E_{VB} - E_g \tag{9}$$

where, E_{VB} and E_{CB} are the valence and conduction band edge potential (w.r.t Normal Hydrogen Electrode (NHE)).

X is the electronegativity of the semiconductor.

E_e is the energy of free electron on hydrogen scale (4.5 eV) and.

E_g is the band gap of the photocatalyst ($BiFeO_3$ ~1.5 eV and $GdFeO_3$ ~ 2.4 eV).

It has been computed that the conduction band (CB) and valence band (VB) potentials of the $BiFeO_3$ are 0.3 eV and 2.3 eV and for the $GdFeO_3$ semiconductor they are 0.5 eV and 2.8 eV, respectively. The reasonable improvement in the photocatalytic properties for BiFeO3 –GdFeO3 nanocomposites can be ascribed to the following three main factors;

Firstly, in the as-prepared $BiFeO_3$ –$GdFeO_3$heterostructures, the $BiFeO_3$ surfaces are not completely covered by $GdFeO_3$, resulting both of them being highly available for the photo absorption and encouraging the formation of depletion layers on the surfaces of both semiconductors when exposed to sunlight. Therefore, $BiFeO_3$ and as well as $GdFeO_3$ are sensitive for light reaction on methylene blue dye molecules.

Secondly, the synthesis of well-distributed heterogeneous photocatalyst could be an efficient way to increase the photocatalytic activity. As such in our work, well-distributed $GdFeO_3$ are decorated perfectly onto the $BiFeO_3$ nanoparticles surface through managing pH = 6.0 so as to keep better electrostatic force of attraction between $BiFeO_3$ and $GdFeO_3$ semiconductors. The $BiFeO_3$ nanoparticles can act as a base for the growth of $GdFeO_3$ nanorods, and avoids the agglomeration of $GdFeO_3$. The smaller $GdFeO_3$ on the $BiFeO_3$ nanoparticles have more exposure and paves way for perfect photon absorption sites to activate and react with dye molecules. Thus, lot of excitations will propagate to the nanocomposite surface, resulting in increased electron extractions from the CB of $BiFeO_3$ nanoparticles. More electron excitations makes the BFO-GFO nanocomposites sensitive to methylene blue dye for the increased response under the visible portion of light.

Thirdly, due to the strong electronic diffusion between $BiFeO_3$ and $GdFeO_3$, a distinct semiconductor junction was formed. Transportation of charge carriers are remarkably enhanced in the hetero-junction, resulting in a quick response. So, $BiFeO_3$–$GdFeO_3$ nanocomposites are better sensitive to methylene blue and have extraordinary properties.

Further, the band gap gets tuned due to the loading $GdFeO_3$ in $BiFeO_3$. Since CB of $GdFeO_3$ are formed above the conduction band in BFO, by increasing the conduction band edge position, it has lead to the reduction of band gap. The electron–hole pair generation inside the conduction band (CB) and valence band (VB) helps to breakdown the organic dye molecules into water molecules (H_2O) and carbon dioxide (CO_2) as by-products under visible light irradiation. The improved photocatalytic activity of $BiFeO_3$ –$GdFeO_3$ is due to the widening of visible light absorption area and improved redox reactions over the photocatalyst surface. The photo-excited BFO-GFO guides the generation of electron–hole pair charge carriers. According to the energy band edge mechanism diagram in Fig. 8, the photo-generated electron in the conduction band of the $BiFeO_3$ will move towards $GdFeO_3$. $GdFeO_3$ (act as strong electron acceptors) inside the $BiFeO_3$ –$GdFeO_3$ matrix acts as the trapping sites for electrons and produce a sufficient separation between charge carriers. It has been reported [55] that the electrons in conduction band of $GdFeO_3$, helps in the reduction of Gd^{3+} into Gd^{2+} species. The Gd^{2+} ions in the photocatalyst surface of can be re-oxidized into Gd^{3+}leads to generation superoxide radical ($\cdot O_2^-$) by reaction with oxygen. Superoxide radical ($\cdot O_2^-$) reacts with water (H_2O) molecules to form Hydroxyl radical ($\cdot$OH). Hydroxyl radicals ($\cdot$OH) and superoxide radicals ($\cdot O_2^-$) are the important candidate to degrade Methylene Blue (MB) into CO_2 and H_2O under visible light irradiation. Similarly, photogenerated holes can migrate from the valence band of $GdFeO_3$ to that of $BiFeO_3$. The movement of photogenerated electron–hole pairs are normally created by the internal electric field. Therefore, the photogenerated electrons and holes could be easily formed at the heterojunction formed between the $BiFeO_3$ and $GdFeO_3$ semiconductors. The series of steps involved in dye degradation are appended here under.

$$BiFeO_3 \xrightarrow{hv} e^- + h^+ \tag{10}$$

$$GdFeO_3 \xrightarrow{hv} e^- + h^+ \tag{11}$$

$$BiFeO_3(e^-)CB \xrightarrow{hv} GdFeO_3(e^-)CB \tag{12}$$

$$GdFeO_3(h^+)VB \xrightarrow{hv} BiFeO_3(h^+)VB \tag{13}$$

$$(h^+)VB + H_2O \rightarrow (\cdot OH) \tag{14}$$

$$(e^-)CB + 0_2\left(\cdot O_2^-\right) + H_2O \rightarrow \cdot OH + OH^- \tag{15}$$

$$\cdot OH + Organic\ pollutant\ (MB) \rightarrow CO_2 + H_2O\ (Degradation\ products) \tag{16}$$

$$(h^+)VB + Organic\ pollutant\ (MB) \rightarrow CO_2 + H_2O\ (Degradation\ products) \tag{17}$$

Thus, the separated electrons and holes charge carriers at the junction region would initiate the degradation of dye reactants on the photocatalyst surface, and leads to the effective photocatalytic activity of $BiFeO_3$ –$GdFeO_3$ nanocomposites.

4. Conclusion

Nanocomposite powders of $BiFeO_3$ –$GdFeO_3$ has been successfully synthesized from sol-gel route without any other impurity phases. The average particle size of composite powders appears to have been increased upon the inclusion of $GdFeO_3$ in the $BiFeO_3$ matrix and it was found to be in the range of 14–35 nm, whereas the parent phases of $BiFeO_3$ and $GdFeO_3$ powders show average crystallite sizes between ~10 – 24 nm. FESEM studies showed that$BiFeO_3$ exists in quasi-spherical structured sheets and $GdFeO_3$ particles appear as the white granular ones. Williamson-Hall strain analysis on nanocomposite powders reveals

the fact that there exists an appreciable change in the crystalline strain upon loading $GdFeO_3$ with $BiFeO_3$ and it fairly agrees with the other results for the possible inclusion of $GdFeO_3$ in the $BiFeO_3$ matrix. UV-Vis-NIR studies on $BiFeO_3$ –$GdFeO_3$ suggest that band gap tuning found to have occurred due to the addition $GdFeO_3$ in the nanocomposite phase. The band gap energies of $BiFeO_3$ –$GdFeO_3$was found as 1.8 eV, whereas the $BiFeO_3$and $GdFeO_3$ figured 2.0 eV and 2.3 eV respectively. The reduction in the band gap energy values of $BiFeO_3$ –$GdFeO_3$ nanocomposites favours for the improved light harvesting property of the nanocomposite phase. FTIR vibrational structure analysis confirm the existence of nanocomposite phase and the vibrations of both moieties do appear in the final compound. Photoluminescence measurements on BFO-GFO composite has shown that there is a reasonable improvement in PL emission at the higher wavelength sire upon loading GFO in BFO and it is attributed to the defect – band transmission. However, it has not affected its photocatalytic activity in visible portions. MB dye degradation activity of $BiFeO_3$ –$GdFeO_3$ nanocomposites shows that the synthesized powder is capable of degrading 98% of dye molecules and converts them as a reusable water, whereas the parent compounds namely $BiFeO_3$ and $GdFeO_3$ found to be capable of degrading 76% and 42% of MB dye. The reusable capacity of the photocatalyst after dye degradation with nanocomposites powders have been ascertained for a consecutive trail of 3 runs. The absorbance values remain invariant. Thus, the obtained nanocomposite powders of BFO-GFO could be a potential candidate for photocatalytic dye degradation applications.

Declarations

Author contribution statement

Yathavan Subramanian: Performed the experiments; Contributed reagents, materials, analysis tools or data.

Venkatapathy Ramasamy: Performed the experiments; Analyzed and interpreted the data; Contributed reagents, materials, analysis tools or data.

R J Karthikeyan, Gokul Raj Srinivasan, Durairajan Arulmozhi: Contributed reagents, materials, analysis tools or data.

Ramesh Kumar Gubendiran: Analyzed and interpreted the data; Contributed reagents, materials, analysis tools or data; Wrote the paper.

Mohan Sriramalu: Conceived and designed the experiments; Analyzed and interpreted the data; Contributed reagents, materials, analysis tools or data; Wrote the paper.

Funding statement

This research did not receive any specific grant from funding agencies in the public, commercial, or not-for-profit sectors.

Competing interest statement

The authors declare no conflict of interest.

Additional information

No additional information is available for this paper.

References

[1] J.G. Yu, J.X. Low, W. Xiao, P. Zhou, M. Jaroniec, Enhanced photocatalytic CO_2-reduction activity of anatase TiO_2 by coexposed {001} and {101} facets, J. Am. Chem. Soc. 136 (2014) 8839–8842.

[2] L. Shang, T. Bian, B. Zhang, D.H. Zhang, L.Z. Wu, C.H. Tung, Y.D. Yin, T.R. Zhang, Graphene-supported ultrafine metal nanoparticles encapsulated by mesoporous silica: robust catalysts for oxidation and reduction reactions, Angew. Chem. Int. Ed. 53 (2014) 250–254.

[3] H.G. Wei, D.W. Ding, X.R. Yan, J. Guo, L. Shao, H.R. Chen, L.Y. Sun, H.A. Colorado, S.Y. Wei, Z.H. Guo, Tungsten trioxide/Zinc tungstate bilayers: electrochromic behaviors, energy storage and electron transfer, Electrochim. Acta 132 (2014) 58–66.

[4] A. Mills, R.H. Davies, D. Worsley, Water purification by semiconductor photocatalysis, Chem. Soc. Rev. 22 (1993) 417–425.

[5] A. Fujishima, K. Honda, Electrochemical Photolysis of Water at a Semiconductor Electrode, Nature 238 (1972) 37–38.

[6] H. Mirabolghasemi, N. Liu, K. Lee, P. Schmuki, Formation of 'single walled' TiO_2 nanotubes with significantly enhanced electronic properties for higher efficiency dye-sensitized solar cells Chem, Commun. Now. 49 (2013) 2067–2069.

[7] H. Irie, K. Kamiya, T. Shibanuma, S. Miura, D.A. Tryk, T. Yokoyama, K. Hashimoto, Visible light-sensitive Cu(II)-grafted TiO_2photocatalysts: activities and X-ray absorption fine structure analyses, J. Phys. Chem. C 113 (2009) 10761–10766.

[8] M. Liu, X.Q. Qiu, M. Miyauchi, K. Hashimoto, Cu(II) oxide amorphous nanoclusters grafted Ti^{3+} self-doped TiO_2: an efficient visible light photocatalyst, Chem. Mater. 23 (2011) 5282–5286.

[9] M.,M. Momeni, Y. Ghayeb, Photochemical deposition of platinum on titanium dioxide–tungsten trioxide nanocomposites: an efficient photocatalyst under visible light irradiation, J. Mater. Sci. Mater. Electron. 27 (2015) 1062–1069.

[10] M.,M. Momeni, Y. Ghayeb, Preparation of cobalt coated TiO_2 and WO_3 –TiO_2 nanotube films via photo-assisted deposition with enhanced photocatalytic activity under visible light illumination, Ceram. Int. 42 (2016) 7014–7022.

[11] Mohamad Mohsen Momeni, Mahboubeh Mirhosseini, Maliheh Chavoshi, Growth and characterization of Ta2O5 nanorod and WTa2O5 nanowire films on the tantalum substrates by a facile one-step hydrothermal method, Ceram. Int. 42 (2016) 9133–9138.

[12] Y. Ghayeb, M.M. Momeni, M. Menati, Reduced graphene oxide/Cu 2 O nanostructure composite films as an effective and stable hydrogen evolution photocathode for water splitting, J. Mater. Sci.: Materials 28 (2017) 7650–7659.

[13] Mohamad Mohsen Momeni, Yousef Ghayeb, Zohre Ghonchegi, Fabrication and characterization of copper doped TiO2 nanotube arrays by in situ electrochemical method as efficient visible-light photocatalyst, Ceram. Int. (2015) 8735, 8735-8714.

[14] Mohamad Mohsen Momeni, Zohre Nazari, Preparation of TiO2 and WO3–TiO2 nanotubes decorated with PbO nanoparticles by chemical bath deposition process: a stable and efficient photo catalyst, Ceram. Int. 42 (2016) 8691–8697.

[15] Mohamad Mohsen Momeni, Ghayeb Yousef, Fabrication and characterization of zinc oxide-decorated titanianoporous by electrochemical anodizing-chemical bath deposition techniques: visible light active photocatalysts with good stability, J. Iran. Chem. Soc. 13 (2016) 481–488.

[16] Mohamad Mohsen Momeni, Mohaddeseh Hakimian, Kazempour Ali, In-situ manganese doping of TiO2 nanostructures via single-step electrochemical anodizing of titanium in an electrolyte containing potassium permanganate: a good visible-light photocatalystCeramics, International 41 (2015) 13692–13701.

[17] Mohamad Mohsen Momeni, Ghayeb Yousef, Preparation of cobalt coated TiO2 and WO3–TiO2 nanotube films via photo-assisted deposition with enhanced photocatalytic activity under visible light illumination, Ceram. Int. (2016) 7014–7022.

[18] Mohamad Mohsen Momeni, Yousef Ghayeb, Zohre Ghonchegi, Visible light activity of sulfur-doped TiO_2 nanostructure photoelectrodes prepared by single-step electrochemical anodizing process, Journal of Solid State19 (2015) 1359–1366.

[19] M.M. Momeni, M. Mirhosseini, M. Chavoshi, A. Hakimizade, The effect of anodizing voltage on morphology and photocatalytic activity of tantalum oxide nanostructure, J. Mater. 27 (2016) 3941–3947.

[20] Mohamad Mohsen Momeni, Study of synergistic effect among photo-, electro-, and sonoprocesses in photocatalyst degradation of phenol on tungsten-loaded titania nanotubes composite electrode, Appl. Phys. A 119 (2015) 1413–1422.

[21] M.M. Momeni, Y. Ghayeb, S. Gheibee, Silver nanoparticles decorated titanium dioxide-tungsten trioxide nanotube films with enhanced visible light photo catalytic activity, Ceram. Int. 43 (2017) 564–570.

[22] Mohamad Mohsen Momeni, Ghayeb Yousef, Synthesis and characterization of iron-doped titania nanohoneycomer5b and nanoporous semiconductors by electrochemical anodizing method as good visible light active photocatalysts, J. Mater. Sci. Mater. Electron. 26 (2015) 5509–5517.

[23] M.M. Momeni, Y. Ghayeb, A.A. Mozafari, Optical and photo catalytic characteristics of Ag 2 S/TiO 2 nanocomposite films prepared by electrochemical anodizing and SILAR approach, J. Mater. Sci. 27 (2016) 11201–11210.

[24] F. Gao, X.Y. Chen, K.B. Yin, S. Dong, Z.F. Ren, F. Yuan, T. Yu, Z.G. Zou, J.M. Liu, Visible-light photocatalytic properties of weak magnetic $BiFeO_3$ nanoparticles, Adv. Mater. 19 (2007) 2889–2892.

[25] U.A. Joshi, J.S. Jang, P.H. Bors, J.S. Lee, Microwave synthesis of single-crystalline perovskite $BiFeO_3$nanocubes for photoelectrode and photocatalytic applications, Appl. Phys. Lett. 92 (2008) 242106.

[26] F. Gao, Y. Yuan, K.F. Wang, X.Y. Chen, F. Chen, J.M. Liu, Preparation and photo absorption characterization of $BiFeO_3$ nanowires, Appl. Phys. Lett. 89 (2006) 102506.

[27] X.Y. Chen, T. Yu, F. Gao, H.T. Zhang, L.F. Liu, Y.M. Wang, Z.S. Li, Z.G. Zou, Application of weak ferromagnetic BiFeO3 films as the photoelectrode material under visible-light irradiation, Appl. Phys. Lett. 91 (2007), 022114.

[28] R.A. He, S.W. Cao, P. Zhou, J.G. Yu, Recent advances in visible light Bi-based photocatalysts, Chin. J. Catal. 35 (2014) 989–1007.

[29] F. Niu, D. Chen, L. Qin, T. Gao, N. Zhang, S. Wang, Y. Huang, Synthesis of Pt/$BiFeO_3$heterostructuredphotocatalysts for highly efficient visible-light photocatalytic performances, Sol. Energy Mater. Sol. Cell. 143 (2015) 386–396.

[30] F. Niu, D. Chen, L. Qin, T. Gao, N. Zhang, S. Wang, Z. Chen, Y. Huang, 'Facile synthesis of highly efficient p–n heterojunction CuO/$BiFeO_3$ composite

photocatalysts with enhanced visible-light photocatalytic activity, ChemCatChem 7 (2015) 3279–3289.
[31] X. Wang, W. Mao, J. Zhang, Y. Han, C. Quan, Q. Zhang, T. Yang, J. Yang, X.A. Li, W. Huang, Facile fabrication of highly efficient g-C_3N_4/BiFeO3 nanocomposites with enhanced visible light photocatalytic activities, J. Colloid Interface Sci. 448 (2015) 17–23.
[32] T. Soltani, B.K. Lee, Sono-synthesis of Nano crystallized $BiFeO_3$/reduced graphene oxide composites for visible photocatalytic degradation improvement of bisphenol A', Chem. Eng. J. 306 (2016) 204–213.
[33] Yathavan Subramanian, Venkatapathy Ramasamy, Ramesh Kumar Gubendiran, Gokul Raj Srinivasan, Durairajan Arulmozhi, Structural, Optical, Thermal and Photocatalytic dye degradation properties of $BiFeO_3$ – WO_3 nanocomposites, J. Electron. Mater. 47 (12) (2018) 7212–7223.
[35] L. Jiang, S. Yang, M. Zheng, H. Chen, A. Wu, Synthesis and magnetic properties of nanocrystalline$Gd_3Fe_5O_{12}$ and $GdFeO_3$ powders prepared by sol–gel auto-combustion method, Mater. Res. Bull. 104 (2018) 92–96.
[36] S. Husain, A.O. A Keelani, W. Khan, Influence of Mn substitution on morphological, thermal and optical properties of nanocrystalline $GdFeO_3$orthoferrite, Nano-Structures & Nano-Objects 15 (2018) 17–27.
[37] V. Bedekar, V. Jayakumar, O.D. Manjanna, A.K. Tyagi, Synthesis and magnetic studies of nano-crystalline $GdFeO_3$, Mater. Lett. 62 (23) (2008) 3793–3795.
[38] X. Li, Z.Q. Duan, Synthesis of $GdFeO_3$ microspheres assembled by nanoparticles as magnetically recoverable and visible-light-driven photocatalysts, Mater. Lett. 89 (2012) 262–265.
[39] E.S. Baeissa, Environmental remediation of aqueous methyl orange dye solution via photocatalytic oxidation using Ag-$GdFeO_3$ nanoparticles, J. Alloy. Comp. 678 (2016) 267–272.
[40] B. Sivakumar, S. Mohan, B. Subramanian, Experimental evidence for the carrier transportation enhanced visible light driven photocatalytic process in bismuth ferrite ($BiFeO_3$) one-dimensional fiber nanostructures, J. Phys. Chem. C 120 (2016) 18811.
[41] S. Bharathkumar, M. Sakar, K. Rohith Vinod, S. Balakumar, Versatility of electrospinning on the fabrication of fibrous mat and mesh nanostructures of bismuth ferrite ($BiFeO_3$) and their magnetic photocatalytic activities, Phys. Chem. Chem. Phys. 17 (2015) 17745.
[42] L. Li, X. Wang, Y. Lan, W. Gu, S. Zhang, Synthesis, photocatalytic and electrocatalytic activities of wormlike GdFeO3 nanoparticles by a glycol-assisted sol–gel process, Ind. Eng. Chem. Res. 52 (2013) 9130–9136.
[43] Jiangtao Wu, Zhaoxiong Xie, Lansun Zheng, Shaoyu Mao, Zuo-Guang Ye, Room-temperature ferromagnetic/ferroelectric $BiFeO_3$ synthesized by a self-catalyzed fast reaction process, J. Mater. Chem. 20 (2010) 6512–6516.
[44] P.D. Dimple, B.P. Mandal, M.D. Mukadam, S.M. Yusufb, A.K. Tyagi, Improved magnetic and ferroelectric properties of Sc and Ticodopedmultiferroicnano $BiFeO_3$ prepared via sonochemical synthesis, Dalton Trans. 43 (2014) 7838.
[45] S. Mathur, H. Shen, N. Lecerf, A. Kjekshus, H. Fjellvag, G.F. Goya, Nanocrystallineorthoferrite $GdFeO_3$ from a novel heterobimetallic precursor, Adv. Mater. 14 (2014) 1405.
[46] V. Mote, Y. Purushotham, B. Dole, Williamson-Hall analysis in estimation of lattice strain in nanometer-sized ZnO particles, Journal of Theoretical and Applied Physics 6 (1) (2016) 6.
[47] D. Moitra, B.K. Ghosh, M. Chandel, N.N. Ghosh, Synthesis of a BiFeO nanowire-reduced graphene oxide based magnetically separable nanocatalyst and its versatile catalytic activity towards multiple organic reactions, RSC Adv. 6 (2016) 97941–97952.
[48] A.A. Kokhanovsky, Physical interpretation and accuracy of the Kubelka–Munk theory, J. Phys. D Appl. Phys. 40 (2007) 2210–2216.
[49] D. Jalandhara, G. Singh, K. Yadav, Effect of Sintering Temperature on the Optical Properties of BiFeO3 Nanoparticles, 2016.
[50] N.D. Ngoc, D.L. Minh, C.P. Ngoc, D.D. Trung, H.C. N Thi, B.N. Quang, L.D. Thi, Low-temperature synthesis and investigations on photocatalytic activity of nanoparticles BiFeO3 for methylene blue and methylene orange degradation and some toxic organic compounds, Adv. Nat. Sci. Nanosci. Nanotechnol. 7 (2016), 045003.
[51] F. Lv, Y. Zhang, X. Chen, Y. Ma, Composition and fluorescence of gadolinium (III) acetylacetonate derivatives by solvothermal method, Int J Opt Photonic Eng 2 (2017) 005.
[52] Geo George Philip, Anitha Senthamizhan, Thirupathur Srinivasan Natarajan, Gopalakrishnan Chandrasekaran, Helen Annal Therese, The effect of gadolinium doping on the structural, magnetic and photoluminescence properties of electrospun bismuth ferrite nanofibers, Ceram. Int. 41 (2015) 13361–13365.
[53] L. Beránek, An examination of the Langmuir-hinshelwood model using ion exchange catalysts, Catal. Rev. 16 (1977) 1–35.
[54] S.G. Bratsch, Revised mullikenelectronegativities: I. Calculation and conversion to pauling units, J. Chem. Educ. 65 (1988) 34.
[55] P. Tang, Y. Hu, T. Lin, Z. Jiang, C. Tang, Preparation of nanocrystalline $GdFeO_3$ by microwave method and its visible-light photocatalytic activity, Integr. Ferroelectr. 153 (2014) 73–78.
[56] D.P. DePuccio, P. Botella, B. O'Rourke, C.C. Landry, Degradation of methylene blue using porous WO3, SiO2–WO3, and their Au-loaded analogs: adsorption and photocatalytic studies, ACS Appl. Mater. Interfaces 7 (3) (2015) 1987–1996.
[57] Yunhui Si, Yayun Li, Jizhao Zou, Xinbo Xiong, Xierong Zeng, Ji Zhou, Photocatalytic performance of a novel MOF/BiFeO3 composite, Materials 10 (2017) 1161.
[58] Abdul Halim Abdullah, Wan Tze Peng, MohdZobir Hussein, Degradation of methylene blue dye by CuO-BiVO4 photocatalysts under visible light irradiation, Malaysian Journal of Analytical Sciences 20 (2016) 1338–1345.